Transition from Unilamellar to Bilamellar Vesicles Induced by an Amphiphilic Biopolymer

Jae-Ho Lee,[1] Vivek Agarwal,[3] Arijit Bose,[3] Gregory F. Payne,[2] and Srinivasa R. Raghavan[1,*]

[1]*Department of Chemical Engineering, University of Maryland, College Park, Maryland 20742-2111, USA*
[2]*Center for Biosystems Research, University of Maryland Biotechnology Institute, College Park, Maryland 20742-4450, USA*
[3]*Department of Chemical Engineering, University of Rhode Island, Kingston, Rhode Island 02881, USA*

(Received 12 August 2005; published 31 January 2006)

We report some unusual structural transitions upon the addition of an amphiphilic biopolymer to unilamellar surfactant vesicles. The polymer is a hydrophobically modified chitosan and it embeds its hydrophobes in vesicle bilayers. We study vesicle-polymer mixtures using small-angle neutron scattering (SANS) and cryotransmission electron microscopy (cryo-TEM). When low amounts of the polymer are added to unilamellar vesicles of ca. 120 nm diameter, the vesicle size decreases by about 50%. Upon further addition of polymer, lamellar peaks are observed in the SANS spectra at high scattering vectors. We show that these spectra correspond to a co-existence of unilamellar and bilamellar vesicles. The transition to bilamellar vesicles as well as the changes in unilamellar vesicle size are further confirmed by cryo-TEM. A mechanism for the polymer-induced transitions in vesicle morphology is proposed.

DOI: 10.1103/PhysRevLett.96.048102 PACS numbers: 87.16.Dg

Biological membranes that enclose cellular organelles are complex mixtures of lipids and amphiphilic macromolecules such as lipoproteins, or transmembrane proteins [1]. The membrane-associated macromolecules perform important biological functions (e.g., recognition and signal transduction), yet it is unclear if they also affect the organelle's size and shape. Several organelles in eukaryotic cells are bilamellar, i.e., have a double membrane structure [1]. These include the nucleus, the mitochondria, and the chloroplasts in plant cells. In these bilamellar organelles, the spacing between the inner and outer membranes appears to be tightly regulated. It is also interesting that the bilamellar organelles coexist within a cell together with numerous unilamellar (single membrane) organelles, such as lysosomes and endosomes [1].

In this Letter, we report the coexistence of unilamellar and bilamellar vesicles in a system consisting of surfactant vesicles and an amphiphilic biopolymer. The biopolymer is a hydrophobically modified chitosan (HM chitosan), obtained by grafting a small number of alkyl tails onto the backbone of the water-soluble polysaccharide, chitosan. Recently [2], we have shown that this HM chitosan can transform a solution of unilamellar surfactant vesicles into an elastic gel. Gelation occurs because hydrophobes on the polymer can insert into adjacent vesicle bilayers and thereby connect vesicles into a three-dimensional network. Similar networking of vesicles by amphiphilic polymers has been reported by others [3–5].

In the present study, we focus on data from these vesicle-HM chitosan mixtures acquired using small-angle neutron scattering (SANS). Based on this data, we report a systematic influence of the polymer on the size and morphology of the vesicles. Specifically, the addition of a small amount of polymer greatly reduces the size of the unilamellar vesicles. On the other hand, at high polymer-to-vesicle ratios, the addition of polymer gives rise to complex SANS spectra with peaks at intermediate values of the scattering vector q. By modeling this data, we demonstrate that it corresponds to a mixture of unilamellar vesicles together with *bilamellar* vesicles, i.e., vesicles with two bilayers. Furthermore, we have corroborated this unusual result by directly visualizing the structure of the vesicles using cryotransmission electron microscopy (cryo-TEM).

The HM chitosan we have used has a molecular weight around 200 000 [2]. It has a hydrophilic backbone due to amine groups, while its hydrophobic character arises from about 25 dodecyl (C12) tails tethered to the backbone at random points (this was done by reacting 2.5 mol % of the amines with a dodecyl aldehyde [6]). Solutions of the HM chitosan were prepared in 1% acetic acid. Under these conditions, the polymer acts as a cationic polyelectrolyte. The vesicles were prepared by mixing solutions of the cationic surfactant, cetyl trimethylammonium tosylate (CTAT) and the anionic surfactant, sodium dodecyl benzene sulfonate (SDBS), in a weight ratio of 70/30. It is well-known that these mixtures spontaneously self-assemble to form unilamellar vesicles with diameters around 100 nm [7,8]. Vesicle-polymer mixtures of desired composition were prepared by mixing the corresponding stock solutions, followed by mild heat.

We present SANS data for vesicle + HM chitosan mixtures in D_2O as a function of polymer concentration [Fig. 1(a)] and vesicle concentration [Fig. 1(b)]. The data were acquired on the NG-1 beamline at NIST in Gaithersburg, MD. The spectra were corrected and placed on an absolute scale using calibration standards provided by NIST and are presented as plots of the absolute intensity I as a function of the scattering vector q. In Fig. 1(a), the vesicle concentration is held constant at 0.5%. Data are shown for the control sample (vesicles, no polymer) and for four different polymer concentrations (the curves are scaled by factors of 10 for clarity). In Fig. 1(b), the polymer concentration is held constant at 0.55%, while the vesicle concentration is varied from 0.2% to 1.4%. The data in

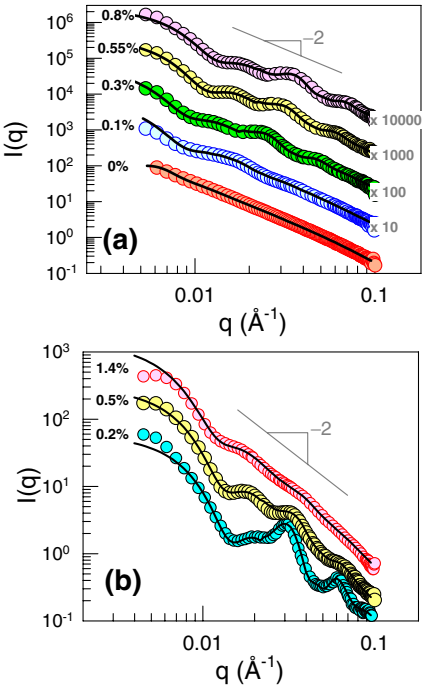

FIG. 1 (color online). SANS data from vesicle-polymer mixtures as a function of (a) the polymer (HM chitosan) concentration and (b) the vesicle concentration. In (a), the vesicle concentration is held constant at 0.5% and data are shown for the polymer concentrations indicated. In (b), the polymer concentration is held constant at 0.55% and data are shown for the vesicle concentrations indicated. Lines through the data are fits to ULV or ULV + MLV models (see text for details).

Fig. 1(b) is shown unscaled—the curves are well separated because the number of scatterers (vesicles) per unit volume is increasing.

We now discuss the interpretation of these spectra. Consider first the control vesicles (Fig. 1). In the dilute, noninteracting limit, the structure factor $S(q) \rightarrow 1$, and so the intensity $I(q)$ is basically given by the form factor $P(q)$ of unilamellar vesicles (ULVs). For vesicles of radius R and bilayer thickness t ($\ll R$), $P(q)$ reduces to [2,9]

$$P(q) = (\Delta\rho)^2 (4\pi R)^2 \frac{t^2}{q^2} \sin^2(qR), \qquad (1)$$

where $(\Delta\rho)^2$ is the scattering contrast. Equation (1) indicates that $I(q)$ should show a q^{-2} decay in the low q range. To account for the polydispersity of the vesicles, we average the form factor over a Schultz distribution, and the spread in vesicle size is quantified by the polydispersity index p [2]. In Fig. 1, the fit from the polydisperse ULV model is shown for the 0.5% vesicle solution. Note that the data follows the expected slope of -2 at low q. The model fit yields three parameters, viz., the average vesicle diameter $\bar{D}$ (117 nm), the bilayer thickness t (2.5 nm), and the polydispersity index p (25%) (see Table I).

Next, we apply the polydisperse ULV model to vesicle-polymer mixtures in cases where the polymer:vesicle ratio is low. For the samples with 0.5% vesicles + 0.1% polymer [Fig. 1(a)] and 1.4% vesicles + 0.55% polymer [Fig. 1(b)], the model yields a very good fit. From the data, we note that the addition of polymer reduces the vesicle size significantly (see Table I). For example, adding 0.1% polymer to a 0.5% vesicle solution reduces the mean vesicle diameter $\bar{D}$ from 117 nm to 53 nm. Such a reduction in ULV size upon addition of polymer was inferred in our previous study as well [2].

TABLE I. Parameters from SANS modeling. For the ULVs, they are the average vesicle diameter $\bar{D}$, the bilayer thickness t, and the polydispersity index p. For the MLVs, they are the d spacing of the bilayers d, the number of bilayer stacks N, and the Caillé parameter η.

Sample	Fit type	ULVs			MLVs		
Ves/Poly(%)		$\bar{D}$ (nm)	t (nm)	p	d (nm)	N	η
0.5/0	ULV	117	2.5	0.25	···	···	···
0.5/0.1	ULV	53	2.5	0.30	···	···	···
0.5/0.3	ULV + MLV	52	2.5	0.30	25.0	2.5	0.50
0.5/0.55	ULV + MLV	40	2.5	0.24	18.4	2.6	0.45
0.5/0.8	ULV + MLV	39	2.5	0.27	17.5	3.0	0.40
0.2/0.55	ULV + MLV	39	2.5	0.21	19.9	3.0	0.29
0.5/0.55	ULV + MLV	45	2.5	0.25	19.9	2.4	0.40
1.4/0.55	ULV	39	2.5	0.30	···	···	···

A further striking feature emerges in the SANS data at higher polymer:vesicle ratios—viz., two peaks at higher values of q, with the peak positions showing a ''lamellar'' spacing (first peak at q_0, second at $2q_0$). We will show that the emergence of these high q peaks implies the formation of multilamellar vesicles (MLVs) with well-defined bilayer spacing. To model a mixed population of ULVs and MLVs, we adopt the following procedure, illustrated in Fig. 2. Two assumptions are inherent to our analysis: (a) the scattering from the two types of vesicles is additive, and (b) the MLVs contribute to the scattering only on account of their bilayers. In other words, the MLVs are assumed to be so large that their overall size falls outside the range probed by SANS, which allows us to neglect their contribution to the scattering at low q.

The data shown in Fig. 2(a) is for the sample with 0.5% vesicles + 0.3% polymer [from Fig. 1(a)]. First, we

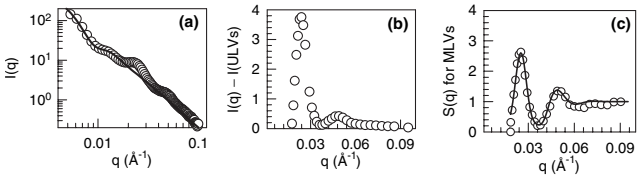

FIG. 2. Typical modeling procedure for data corresponding to a mixture of ULVs and MLVs. The sample is a mixture of 0.5% vesicles and 0.3% HM chitosan. (a) The low q data is fit to a ULV model. (b) The difference between the overall data and the ULV model is shown. (c) The structure factor contribution to the curve in (b) is shown, and the line through this data is a fit to the Nallet model [Eq. (3)].

apply the ULV model to the low-q data, ignoring the high-q peaks. Note that the fit is excellent at low-q, and it gives an average vesicle diameter of 52 nm (Table I). Next, we subtract the ULV fit from the total intensity, and the resulting data is shown in Fig. 2(b). This data corresponds to the MLVs, and it closely resembles the scattering from a lamellar phase, with peaks at q_0 and $2q_0$. To model this data, we use the approach of Nallet *et al.* [10], who have developed analytical expressions for the form and structure factors of a stack of bilayers. The two parameters in their model are the number of bilayer stacks N and the Caillé parameter η (which is inversely related to the bilayer rigidity) [10,11]. A third parameter, the d spacing of the bilayers, is obtained independently from the peak position ($d = 2\pi/q_0$). In the Nallet model, the bilayer form factor $P_B(q)$ is given by the equation below (the bilayer thickness t is assumed to be that of the ULVs) [10]:

$$P_B(q) = \frac{2\Delta\rho^2}{q^2}\left[1 - \cos(qt)\exp\left(-\frac{q^2t^2}{32}\right)\right]. \quad (2)$$

The total intensity in Fig. 2(b) divided by $q^{-2} \cdot P_B(q)$ represents the structure factor $S_B(q)$ for bilayers, which is normalized such that it asymptotes to 1. These data are then fit to the following expression for $S_B(q)$ due to Nallet *et al.*, which is valid for a small number of bilayer stacks N [10]:

$$S(q_z) = 1 + 2\sum_{1}^{N-1}\left\{\left(1 - \frac{n}{N}\right)\cos(nq_zd)\exp\left(-\frac{\eta n^2 q_z^2 d^2}{16}\right)\right\}, \quad (3)$$

where $q_z = q - q_0$. From the fit, the two parameters N and η are extracted and their values are given in Table I for the various samples. The values of the stack number N range from 2.4 to 3; the fractions represent linear combinations of the above model for the integral values of $N = 2$ and 3. This implies that there are between two and three bilayers in each of our MLVs, which is corroborated below by our cryo-TEM studies.

Cryo-TEM analysis of our samples was performed using a JEOL 1200EX TEM. Sample preparation was done as follows [12]: first, a drop of the sample was placed on a holey carbon film supported on a TEM grid. A filter paper was then used to blot the drop so as to create a thin film. The grid was then plunged into liquid ethane to rapidly vitrify the sample. Thereafter, the grid was transferred to the TEM for observation at $-170\,^{\circ}$C. Typical images of our samples are shown in Fig. 3. As expected, the control CTAT/SDBS sample shows polydisperse unilamellar vesicles, with diameters ranging from 60–100 nm. However, in the 0.5% vesicles + 0.3% HM chitosan sample, two types of vesicles are seen. On the one hand, there are a number of ULVs with diameters ranging from 20 to 60 nm. In addition, there are also larger bilamellar vesicles (BLVs), i.e., vesicles with two concentric bilayers, with diameters exceeding 100 nm. A similar mixture of

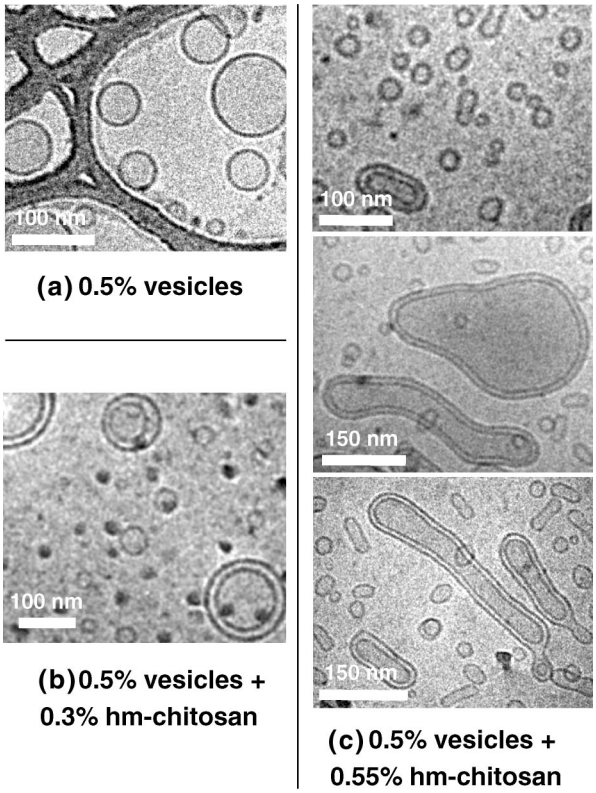

FIG. 3. Cryo-TEM images of the control vesicles (a) and vesicle-polymer mixtures (b), (c). Samples (b) and (c) show a coexistence of unilamellar vesicles (which are smaller than the control case) and bilamellar vesicles.

ULVs and BLVs are seen in the three images of the 0.5% vesicles + 0.55% HM chitosan sample. Again, the ULVs are quite small (20–50 nm diameter) compared to the BLVs. A number of the BLVs are seen to be elongated structures—this may be a result of the shear caused by the blotting during sample preparation [13]. We should emphasize that mixtures of ULVs and BLVs were seen in virtually all images collected for this sample.

It is significant that the cryo-TEM images reinforce the conclusions obtained from SANS modeling. Specifically, the images confirm that (i) adding polymer reduces the sizes of the ULVs relative to the control vesicles, and (ii) at higher amounts, the polymer also induces the formation of BLVs that coexist with the ULVs. Because of the shear associated with cryo-TEM sample preparation, a more quantitative comparison between the SANS and cryo-TEM data is not possible. Nevertheless, the qualitative agreement is encouraging.

Further insight into our system can be obtained from the trends in parameters obtained from SANS modeling. First, at a constant vesicle concentration of 0.5%, the d spacing between the bilayers in the MLVs steadily decreases with increasing polymer concentration (Table I). Second, the Caillé parameter η shows a systematic decrease from around 0.8 to a plateau around 0.4 with increasing polymer:vesicle ratio (this is reflected as a

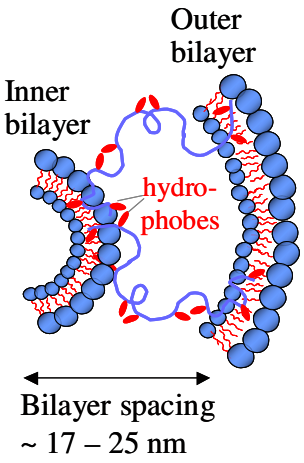

FIG. 4 (color online). Schematic of the concentric bilayers in the bilamellar vesicles. The polymer is visualized as spanning the bilayers with hydrophobes inserted into each one. The bilayer spacing is a function of the polymer concentration.

sharpening of the SANS peaks). η is inversely related to the product of the bending modulus κ and compression modulus B of the bilayers [10,11]. Thus, η is an inverse measure of bilayer rigidity, and a decrease in η implies a stiffening of the bilayers. Also, as noted above, the number of bilayer stacks N shows a small but systematic increase with increasing polymer:vesicle ratio, inching closer to 3 at high ratios. Finally, with regard to the size of the ULVs present, the average ULV diameter decreases to ca. 40 nm upon adding just a small amount of polymer and remains around this value with further polymer addition.

Based on these trends, we can suggest a tentative mechanism to explain the structural changes. At low amounts of HM chitosan, the vesicles are decorated with a few HM chitosan chains that have inserted some of their hydrophobes into the vesicle bilayers. These chains extend between adjacent vesicles and thereby connect and network these vesicles. On account of the embedded polymer chains, the bilayer becomes more rigid, which explains the decrease in η [11]. In turn, the increase in bilayer rigidity serves to stabilize a higher curvature for the vesicles, as has been observed by others [8]. This can explain why the average vesicle size decreases. As more polymer is added, there is an increase in the number of polymer chains bound to vesicles, as well as an increase in connections between adjacent vesicles. The vesicle size cannot drop indefinitely (a limiting curvature is apparently reached when the diameter falls to ca. 40 nm); so, a different scenario is initiated. The polymer chains connecting adjacent ULVs induce their fusion into bilamellar structures having inner and outer membranes (Fig. 4). Each BLV is evidently formed from several smaller ULVs, with the polymer chains bridging the two bilayers. At the onset of BLV formation, the spacing between the bilayers in the BLVs is comparable to the polymer's radius of gyration (ca. 30 nm) [2]. With further polymer addition, the bilayer spacing systematically decreases—presumably, this is because bilayers that are covered by polymer chains to a greater extent experience an attractive "pull" towards each other. In other words, by bringing the bilayers closer, the polymer chains maximize the favorable contact between their hydrophobes and the confining bilayers, even if the chains have to sacrifice some configurational entropy.

In conclusion, we have shown in this Letter that the addition of a hydrophobically modified biopolymer to ULVs can induce the fusion of some of these structures to form BLVs. These structures have been directly visualized by cryo-TEM. Moreover, the coexistence of unilamellar and bilamellar vesicles in the sample leads to a striking pattern in SANS with multiple peaks, and modeling of this SANS data corroborates such a vesicular coexistence. Finally, we should point out that our samples with coexisting ULVs and BLVs appear to be quite stable. No phase separation is observed in these samples over more than a year. Moreover, SANS data on the same sample taken a year apart are nearly identical [14]. This gives credence to the idea that the structural transitions reported here are indeed driven by changes in membrane rigidity and curvature.

This work was funded by the NSF-MRSEC at UMD. We thank NIST for facilitating the SANS experiments.

*Corresponding author.
Email address: sraghava@eng.umd.edu

[1] B. Alberts, *Molecular Biology of the Cell* (Garland Publishers, New York, 2002).
[2] J. H. Lee, J. P. Gustin, T. H. Chen, G. F. Payne, and S. R. Raghavan, Langmuir **21**, 26 (2005).
[3] W. Meier, J. Hotz, and S. Gunther Ausborn, Langmuir **12**, 5028 (1996).
[4] E. F. Marques, O. Regev, A. Khan, M. D. Miguel, and B. Lindman, Macromolecules **32**, 6626 (1999).
[5] H. S. Ashbaugh, K. Boon, and R. K. Prud'homme, Colloid Polym. Sci. **280**, 783 (2002).
[6] J. Desbrieres, C. Martinez, and M. Rinaudo, Int. J. Biol. Macromolecules **19**, 21 (1996).
[7] E. W. Kaler, A. K. Murthy, B. E. Rodriguez, and J. A. N. Zasadzinski, Science **245**, 1371 (1989).
[8] H. T. Jung, B. Coldren, J. A. Zasadzinski, D. J. Iampietro, and E. W. Kaler, Proc. Natl. Acad. Sci. U.S.A. **98**, 1353 (2001).
[9] T. Zemb and P. Lindner, *Neutron, X-Ray and Light Scattering* (Elsevier, Amsterdam, 1991).
[10] F. Nallet, R. Laversanne, and D. Roux, J. Phys. II **3**, 487 (1993).
[11] B. S. Yang, J. Lal, P. Richetti, C. M. Marques, W. B. Russel, and R. K. Prud'homme, Langmuir **17**, 5834 (2001).
[12] I. I. Yaacob and A. Bose, J. Colloid Interface Sci. **178**, 638 (1996).
[13] D. Danino, Y. Talmon, and R. Zana, Colloids Surf. A **169**, 67 (2000).
[14] J.-H. Lee, Ph.D. Dissertation, University of Maryland, 2006.